encit 2020

ABCM Associação Brasileira de Engenharia e Ciências Mecânicas

18th Brazilian Congress of Thermal Sciences and Engineering
November 16-20, 2020 (Online)

ENC-2020-0371
UNBALANCED FREE TO OSCILLATE TANDEM CYLINDERS IN A TURBULENT CROSSFLOW

Patrick Batista Habowski
Guilherme Henrique Fiorot
Universidade Federal do Rio Grande do Sul, Programa de Pós-Graduação em Engenharia Mecânica (PROMEC/UFRGS), Rua Sarmento Leite, 425, Porto Alegre, CEP 90050-170, Brazil.
patrick.habowski@ufrgs.br (P.B. Habowski), guilherme.fiorot@ufrgs.br (G.H. Fiorot)

Alexandre Vagtinski de Paula
Universidade Federal do Rio Grande do Sul, Departamento de Engenharia Mecânica (DEMEC/UFRGS), Rua Sarmento Leite, 425, Porto Alegre, CEP 90050-170, Brazil
depaula@ufrgs.br

Sergio Viçosa Möller
Universidade Federal do Rio Grande do Sul, Programa de Pós-Graduação em Engenharia Mecânica (PROMEC/UFRGS), Rua Sarmento Leite, 425, Porto Alegre, CEP 90050-170, Brazil.
svmoller@ufrgs.br

Abstract. *This article presents an experimental study in an aerodynamic channel using two circular cylinders in tandem position. The two cylinders are positioned between two circular tables aligned with the walls of an aerodynamic channel. The first cylinder is centered while the second is positioned at a distance given by a p/d spacing ratio = 1.26. The set shaft is provided with low friction bearings. When subjected to a transversal flow, the set aligns in a tandem configuration with the flow and begins to oscillate. Hot wire anemometry technique was employed with the wavelet analysis to evaluate the results of velocity and energy content of the wake flow. The angular movement of the system was analyzed using a high-speed camera. Matlab and Tracker software were used to generate time series of the angular position of the cylinder oscillation. Time series of three proposed cases of velocity and angular position were analyzed. In each case, three velocities were imposed. Two cases involved the insertion of obstacles to accelerate the flow close to the cylinders, while the remaining one was carried out without obstacles. Results showed velocity fluctuations due the oscillatory movement developed by the setup, presenting higher levels of velocity for the cases with obstacles. The energy content analysis presented higher levels of energy where the experiment has the higher levels of velocity and velocity fluctuations. Angular position analysis pointed out the oscillatory movement developed by all the three cases.*

Keywords: *Aerodynamic channel, Hot wire anemometry, Tandem cylinders, Turbulent flow, Wavelets.*

1. INTRODUCTION

Circular cylinders can be seen as simplified structures from more complex structures employed in engineering applications, as pipelines, bridge and bridge structures, transmission lines, etc.; rows and arrays of cylinders are employed as well, as in the case of the nuclear reactors, heat exchangers, steam generation, etc. This simplification is interesting to study phenomena that occur in these structures; some examples are boundary layer, vibration and noise. The flow around tubes is complex and irregular, having no complete analytical modeling (Endres and Möller, 2001), being important and suitable the study of this structures in a simplified form.

Interactions between circular cylinders have been studied in the last three decades (e.g., Blevins, 1990, Gu, 1996, Alam and Sakamoto, 2005, De Paula et al., 2012, Woyciekoski et al., 2020). The main characteristic observed in these experiments is the presence of two asymmetric wakes downstream the cylinders, one wide and other narrow, that randomly alternates between the cylinders. This phenomenon, known as bistability, influences the drag coefficients due the asymmetry of the wakes behind the cylinders. Moreover, the phenomenon also does not present symmetry along the z-axis (Alam et al., 2003, Neumeister et al., 2018), increasing its complexity.

Cylinders placed in staggered configurations, forming an angle with the flow, can be summarized by the studies of Sumner et al. (1997), Sumner et al. (1999), Sumner et al. (2000), Habowski et al. (2019) and Habowski et al. (2020). This kind of arrangement forms two asymmetric wakes that, in general, do not present the bistable flow phenomenon. Therefore, since these two wakes present different drag coefficients, a resulting torque is applied in the setup; depending

on the flow velocity, this configuration leads the setup to oscillate and, in some cases, to rotate the setup (Varela et al., 2017).

The fixed tandem positioning presents the formation of one wake, with low velocities values comparing with the free-flow, about 15% of the main flow (Habowski, 2020). According to Zhou and Alam (2016), the tandem position presents interference due the wakes and proximity of the cylinders; this depends on the distance between the cylinders. Also, at least five types of interactions between the wakes were observed.

In general, the flow around two tandem cylinders with equal diameters is classified into three regimes (Zdravkovich, 1987): the first one, called as the extended body regime, where the flow in the gap of the cylinders is stagnant and the cylinders are close enough that the free shear layers separated from upstream cylinder exceed the downstream cylinder; the second one, called as reattachment regime, where the shear layers separated from the upstream cylinder reattach on the downstream cylinder and the gap flow is insignificant yet; the third one, called as co-shedding regime, where the shear layers roll up alternately in the gap between the cylinders and the gap flow is now significant.

In the literature for two tandem cylinders, not only the subcritical regime but also laminar/early turbulent (Re number from $10^2 - 10^3$) and supercritical regimes (Re number $> 1.5 \times 10^5$) are also explored. Papaioannou et al. (2006) presented two and three-dimensional numerical study for two tandem cylinders in laminar/early turbulent regime. Authors showed that 2D numerical results diverged from 3D ones as the Reynolds number is increased (Re ~ 500), indicating three-dimensional effects significantly interferes in the flow around cylinders. Regarding supercritical regime, one of the main objectives is to analyze the noise generated in two tandem cylinders as present Jenkins et al. (2006). The authors employed hot wire anemometry technique together with Particle Image Velocimetry (PIV) and observed the vortex shedding in the near-wake region and high unsteady pressure in the gap region.

An extensive study for fixed tandem cylinders in subcritical regime was presented by Alam and Zhou (2008). In their exploration, the authors performed experiments with two cylinders: the downstream cylinder have a fixed diameter (D) and the upstream cylinder diameter was varied from $0.24D$ to D. The Strouhal number, forces and flow structures around the cylinders were evaluated. Two distinct vortex frequencies were detected behind the downstream cylinder for the case in which the cylinders had the same diameter. Also, the time-averaged drag on downstream cylinder increased with the reduction of the upstream cylinder diameter. On the other hand, the fluctuating forces decreased with the reduction of the upstream cylinder diameter.

It is well established that the main phenomenon of interest when studying cylinders in tandem position is the induced vibrations caused by this configuration (Papaioannou et al., 2008; Bao et al., 2012; Qin et al., 2017), which occur even for cylinders with different diameters. In fact, the vibrations generated in this configuration may cause damages to the structures themselves (Chen, 1985, 1987, Païdoussis, 1980, 1982), and can also produce undesired noise (Jenkins et al., 2005; Lockard et al., 2007). This means that vibration and noise must be taken into account during the projects of buildings and airplanes, for example, showing its importance for engineering applications.

In this way, this article presents an experimental study, where two circular cylinders were tandem placed with a p/d ratio equal to 1.26 inside an aerodynamic flow channel. The cylinders setup is submitted to a transversal and turbulent flow, where the cylinders are free to oscillate. The results of velocity, energy content and angular position behavior were measured by hot wire anemometry technique and explored by means of wavelet analysis and assist of a high-speed camera. Matlab and Tracker software were employed to perform the mathematical analysis.

2. MATHEMATICAL BACKGROUND: WAVELET AND TIME-DOMAIN ANALYSIS

In the study of random processes and phenomena, the Fourier analysis is one of the most common mathematical techniques available for application. However, considering the turbulent flow or possible bistable flow phenomenon and its non-ergodicities, the wavelet analysis arises as the most suitable mathematical tool for such cases (De Paula et al., 2013, Indrusiak et al., 2016).

The wavelet analysis allows the study of a non-stationary and non-ergodic signal in frequency and time domains. The detection of non-permanent structures is also possible throughout such mathematical tool. The main mechanism of this analysis is the stretching and compressing of the window of Fourier transform. In this way, the scales of interest in time and frequency domains are defined (Percival and Walden, 2000).

The Continuous Wavelet Transform (CWT) function is presented in Eq. (1). The wavelet spectrum is defined by the matrix of squared wavelets coefficients, given by Eq. (2). In the wavelet spectrum, the energy is related to time and frequency variables, allowing the representation of the energy over time and frequency domains at same time, which is suitable to the study of transient signals. The Discrete Wavelet Transform (DWT) is a sub sampling of CWT, dealing with dyadic scales. Through the DWT analysis, the energy of time series signal is decomposed in the respective scales, given by Eq. (3). Finally, any discrete time series with defined sampling frequency (Fs) can be represented by Eq. (4), where the first term is the approximation of the signal at scale J, corresponding to the frequency interval $[0, Fs/2^{J+1}]$, and the second term is the high frequency composition of the signal of scales j, where $1 < j < J - 1$, corresponding to the frequency intervals $[Fs/2^{j+1}, Fs/2^{j}]$. In the present work, we used Db20 wavelet and a level 8 ($J = 8$) to reconstruct the signals. All coefficients and variable are detailed in Table 1.

$$\tilde{X}(a,b) = \int_{-\infty}^{+\infty} x(t)\psi_{a,b}(t)\,dt \quad a,b \in \Re \tag{1}$$

$$P_{xx}(a,b) = \left|\tilde{X}_{a,b}\right|^2 \tag{2}$$

$$\tilde{X}(j,k) = \sum_t x(t)\,\psi_{j,k}(t) \quad j,k \in \Re \tag{3}$$

$$x(t) = \sum_k \tilde{X}(J,k)\phi_{J,k}(t) + \sum_{J\leq 1}\sum_k \tilde{X}(j,k)\phi_{J,k}(t) \tag{4}$$

The time-domain analysis is a mathematic tool used to perform the statistical study of obtained data. It is common to compute the mean value of the signal and the standard deviation. However, in this study, it was also computed the skewness (S_k) and the flatness (K) of the signal. According to Tennekes and Lumley (1972), the skewness is a dimensionless measure of the asymmetry of the signal, given by Eq. (5). It indicates the strength and direction of the asymmetry. The flatness is related to the values which are distant from the mean value. Equation (6) describes the dimensionless measure of flatness. The used coefficients and variables are detailed in Table 1.

$$S_k = \frac{\int_{-\infty}^{\infty} u'^3\ B(u')du'}{\sigma^3} \tag{5}$$

$$K = \frac{\int_{-\infty}^{\infty} u'^4\ B(u')du'}{\sigma^4} \tag{6}$$

Table 1 - Description of each coefficient and variable presented in Equations 1 − 6.

Coeff./Var.	Description	Coeff./Var.	Description
$\tilde{X}(a,b)$	generic function in the wavelet domain	$\phi_{J,k}(t)$	scaling function associated to the wavelet function
a,b	wavelet parameters	*J*	reconstruction level
x(t)	generic function in the time domain	S_k	Dimensionless measure of skewness
$\psi_{a,b}(t)$	generic wavelet function	*K*	Dimensionless measure of flatness
$P_{xx}(a,b)$	wavelet spectrogram	u'	velocity fluctuations
$\tilde{X}(j,k)$	wavelet series for the given *j* and *k* coefficients	$B(u')$	Probability Density Function of u'
j,k	dilatation and translation coefficients, respectively	σ^3	square root cube of the standard deviation
$\psi_{j,k}(t)$	generic wavelet function	σ^4	fourth square root power of standard deviation

3. EXPERIMENTAL METHODOLOGY

This study was carried out in the Laboratory of Fluid Mechanics from Universidade Federal do Rio Grande do Sul (LMF – UFRGS). An aerodynamical channel was used to obtain the results of velocity series operating with air as work fluid. The channel has a rectangular cross-section of 193 × 146 mm (width × height) and is 2.29 m long, built in commercial acrylic glass due its smoothness and transparency (Figure 1). A centrifugal blower drives the air from the surroundings, where the temperature and pressure are recorded. After passing through the centrifugal blower, the air goes through a diffusor, two honeycombs and two screens, to reduce the turbulence intensity in the middle of the test section to about 1% of the free-flow stream. Then, the air flow passes through the experimental setup and, finally, to the acquisition data system. A section with a Pitot tube and a static pressure tap connected to a pressure transductor is located upstream the cylinders, where the free-flow velocity is measured. A temperature probe is also located in this section to measure the temperature of the air inside the aerodynamic channel.

The acquisition system is a DANTEC StreamLine constant hot wire anemometry (CTA) system. One hot wire probe, type DANTEC 55P11, designed with a single wire perpendicular to the flow, is placed downstream the cylinders and connected to the CTA system. The data is acquired by a 16–bit A/D board, with USB interface. The sampling frequency was set 1000 Hz during the experiments, with a low pass filter with cutoff frequency set at 300 Hz. The number of data points collected was 32,768 samples, which leads an experiment duration of 32.768 s.

For this study, two circular cylinders of 25.1 mm of diameter were employed. The cylinders are made of commercial PVC (Polyvinyl Chloride) and were mounted in two circular tables 3D printed. These tables have a centralized pin in the

downside and lugs in the upside, where the cylinders are docked. In this configuration, one cylinder is located exactly in the center of the table and the other is located close to the border. This mounting was then placed inside the aerodynamic channel, fixed in low wear bearings (the damping in the system was not accounted in this study). A pointer, fixed in the pin, was placed to identify the angular position of this system during the experiment (Figure 2a). The hot wire anemometer was positioned 18 mm from the center of the downstream cylinder, aligned with it (Figure 2b). The relation *p/d* for this experiment was 1.26, where *d* is the cylinder diameter and the *p* (pitch) is the distance between the center of the cylinders.

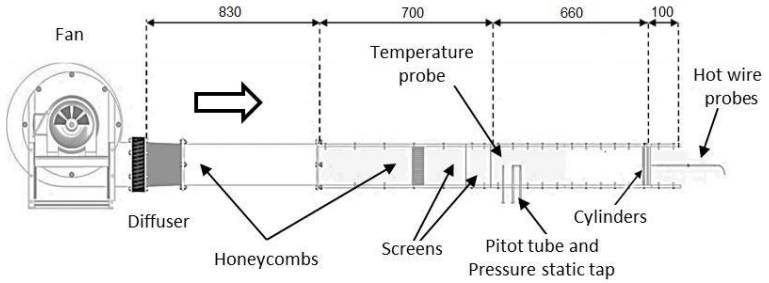

Figure 1 – Schematic of the aerodynamic channel [mm].

This study explored three values for free-flow velocities: 5, 7.5 and 10 m/s. For these cases, the Reynolds numbers were computed based on the cylinder diameter and considering the air conditions in the moment of the experiment are 8.47×10^3, 1.27×10^4 and 1.66×10^4, respectively. In the rest position (0°), the setup is perpendicularly aligned to the flow. This setup leads a blockage ratio varying between 13% to 26% (rest position to maximum angular position possible).

Besides the velocity variation, three different geometric configurations of the aerodynamic channel were carried out. The first case, called no obstacles case, was the reference case, in the configuration explained before, where measures were taken after the turning on of the blower. The second and third cases, called as one obstacle and two obstacles, respectively, consisted on modifying the geometry of the channel placing one/two "throat devices" upstream the cylinders, in order to directing the flow against the setup of the cylinders (Figure 2c and d). For second and third cases had blockage ratio of 38 – 51% and 64 – 77%, respectively. A summarization of the studied cases is presented in Table 2.

Table 2 - Summarization of studied cases.

Studied case/ Info	**No obstacles case**	**One Obstacle**	**Two obstacles**
U_{ref} [m/s]	5, 7.5 and 10	5, 7.5 and 10	5, 7.5 and 10
Re numbers	8.47×10^3, 1.27×10^4 and 1.66×10^4, respectively.	8.47×10^3, 1.27×10^4 and 1.66×10^4, respectively.	8.47×10^3, 1.27×10^4 and 1.66×10^4, respectively.
Throat dev. [un.]	-	One device	Two devices
Blockage ratio [%]	13 − 26	38 − 51	64 − 77
Figure for reference	-	Figure 2 (c)	Figure 2 (d)

The movement of the cylinders setup was studied using a high–speed camera model Phantom V411 – Ametek, equipped with a 50 mm lens model AF–S VR Micro–Nikkor, with a resolution of 640 x 480 pixels, operating at 1000 frames per second, which corresponds to the 1 kHz frequency in the data acquisition of the hot wire signal. The camera was conveniently positioned using a tripod and controlled by a computer connected to the camera with an Ethernet cable. The synchronization between the velocity signal and the camera was performed by the CTA controller, which controls the anemometer system and owns an auxiliary output signal used to trigger the recording. A mirror was mounted at the top of the flow channel, positioned 45° with the camera, in order to track the angle between the cylinders and the main flow. A white background was place behind the pointer to enhance the contrast for the posterior video analysis. A scheme with the detailed positioning about the channel and the high-speed camera is presented in Figure 2 (e).

Wavelet analysis for the hot wire anemometer signals and the video analysis was performed using the Matlab. The wavelet analysis was performed through the specific Matlab toolbox, which is a resource of the software that allows the application of continuous and discrete wavelets to the data analyzed. The Tracker software was employed to track a physical point at each time step during the experiment by properly identifying a feature in the images recorded. After processing the images, a file containing the data of time and angular position was exported by the software, which can be read by Matlab software. The estimated mean error for the angular position is 0.0239 rad.

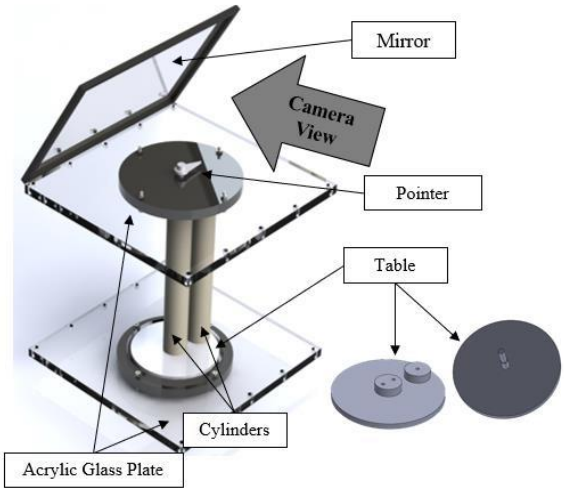

(a)

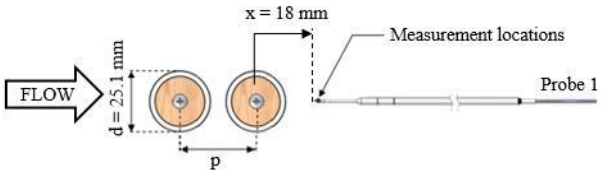

(b)

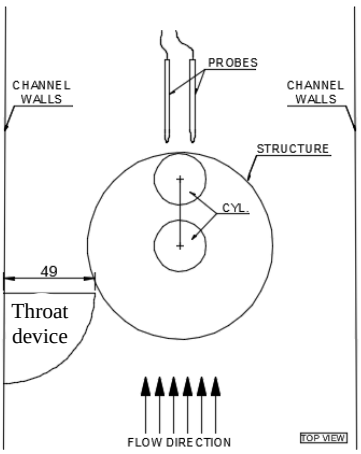

(c)

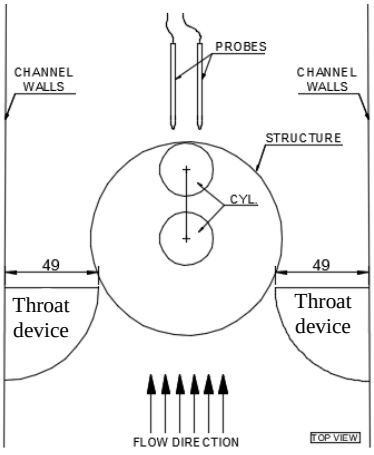

(d)

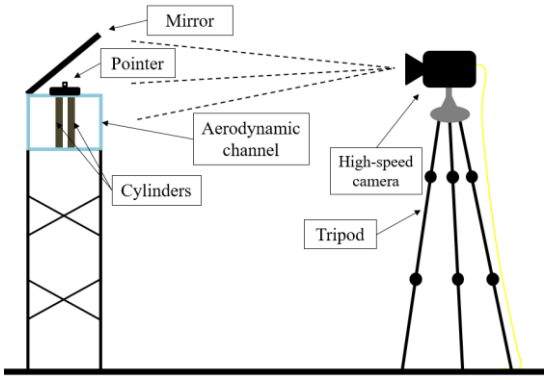

(e)

Figure 2 – Summarized view of the setup (a). Hot wire anemometers position details for all the cases explored (b). Details for the "throat devices" mounted inside the channel (c and d). Front view of the experiment: aerodynamic flow channel plus the setup of the cylinders and the mirror at the top (left); camera positioned (right) for the experiments (d).

4. RESULTS

This section presents the results for each velocity in combination with each geometry, leading to a total of nine experimental runs. The first subsection discusses the velocity series obtained from the hot wire anemometers technique. The second subsection presents an analysis of the energy content of the velocity signals by means of continuous wavelet analysis. In the last subsection, the angular position of the setup is explored based on the results of the recordings and Tracker software analysis.

4.1 Velocity series results

The results for the velocity series from the hot wire anemometers technique, for each proposed case and velocity, are presented in Figure 3. For each chart in Figure 3, the velocities series and its reconstruction by means of discrete wavelet transform were plotted together. The wavelet Db20 type with level 8 of reconstruction ($J = 8$) was employed to reconstruct the signals, generating a reconstructed signal from 0 to 3.9063 Hz.

The blower was turned on while the data started to be acquired. Thus, it can be seen in Figure 3 that the flow starts from rest and begins to accelerate at 4 s. This is a characteristic due the methodology employed. The velocity increased until the moment when several oscillations in the velocity values start to appear. From the moment these oscillations were present, they remained for the rest of the experiment. This oscillation in velocity values is due the angular behavior of the setup (see section 4.3) and are clearly presented for the second and third cases (Figure 3 d–i). These two cases were the experiments which presented the highest levels of velocity.

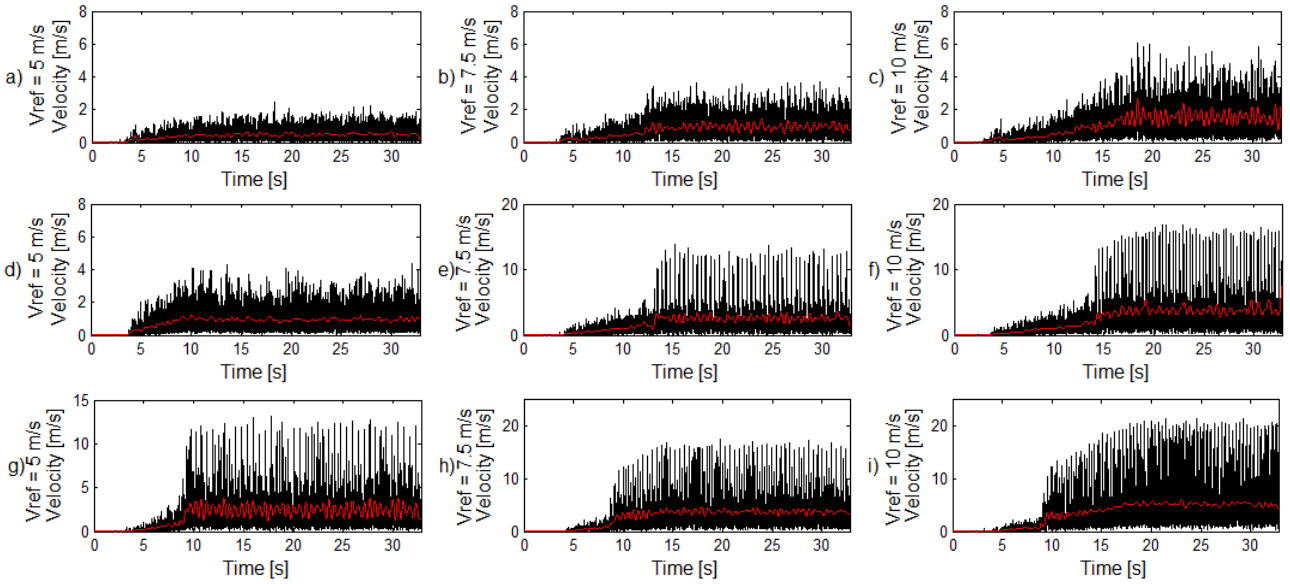

Figure 3 – Data for the velocity measured through hot wires anemometers and respective DWT signals in different configurations. No obstacles case for 5 m/s (a), 7.5 m/s (b) and 10 m/s (c). One obstacle case for 5 m/s (d), 7.5 m/s (e) and 10 m/s (f). Two obstacles for 5 m/s (g), 7.5 m/s (h) and 10 m/s (i). (black line: velocity series, red line: DWT)

Using the velocities signals and the time-domain analysis, results for mean velocity, maximum velocity, standard deviation, skewness and flatness are presented in Table 3. From Figure 3a-c and Table 3, the no obstacles case presents the lowest values of mean and maximum velocities and almost no oscillations are perceived for 5 m/s (Figure 3a). On the other hand, for free-flow velocity of 7.5 and 10 m/s, results present a seemingly increase in oscillations. As expected, the addition of the obstacles and consequently the increase in the blockage ratio increased the mean and maximum velocities of the experiments with one and two obstacles.

The oscillations in the signals can be analyzed using the values of standard deviation, skewness and flatness presented in Table 3. The standard deviation is a simple form to analyze the oscillations presented in the signal. In all studied cases, the standard deviation increased together with the increase in free-flow velocity, which represents how the amplitude of oscillations increases. The skewness values are positive, indicating the existence of an asymmetry in the velocity values caused by the oscillations previously observed in Figure 3. The one obstacle case presented the highest values for skewness, slightly higher than the two obstacles case. This fact may be caused by the deviated flow against to the side of the cylinders, increasing the velocity oscillations. Computed flatness for the same test presented the highest observed value. This could be explained by the fact that the oscillations for the one obstacle case to be much higher than the mean value of velocity. Results for flatness in no obstacles case presented the lowest values, mainly because oscillations presented low amplitudes. Still, all free-flow velocities in two obstacles case presented high values of flatness in comparison of the other cases, even for 5 m/s.

Table 3 - Statistical analysis from velocity signals for all explored cases.

Case	Flow Vel. [m/s]	Mean [m/s]	Max. [m/s]	Std. dev. [m/s]	Skewness	Flatness
No obstacles	**5**	0.390	2.474	0.324	1.176	4.417
	7.5	0.684	3.687	0.611	1.126	3.939
	10	0.999	6.059	0.946	1.251	4.357
One Obstacle	**5**	0.789	4.366	0.598	0.969	4.255
	7.5	1.801	13.865	2.149	2.418	9.413
	10	2.434	16.823	3.029	2.311	8.284
Two Obstacles	**5**	1.872	13.174	2.069	2.193	8.521
	7.5	2.712	17.505	2.924	2.114	8.362
	10	3.467	21.506	3.765	2.072	8.164

4.2 Energy content analysis

The energy content results are presented in Figure 4, by means of the continuous wavelet transform (CWT). The wavelet Db20 type was used to generate the plots, with a bandwidth of 1 Hz. Together with the energy content, the DWT

for velocity results were also brought. The reddish colors mean high energy content, and, the bluish colors, low energy content. The frequency range in the y-axis was adjusted according the experiment, as well the scale of velocity (DWT) in the right side.

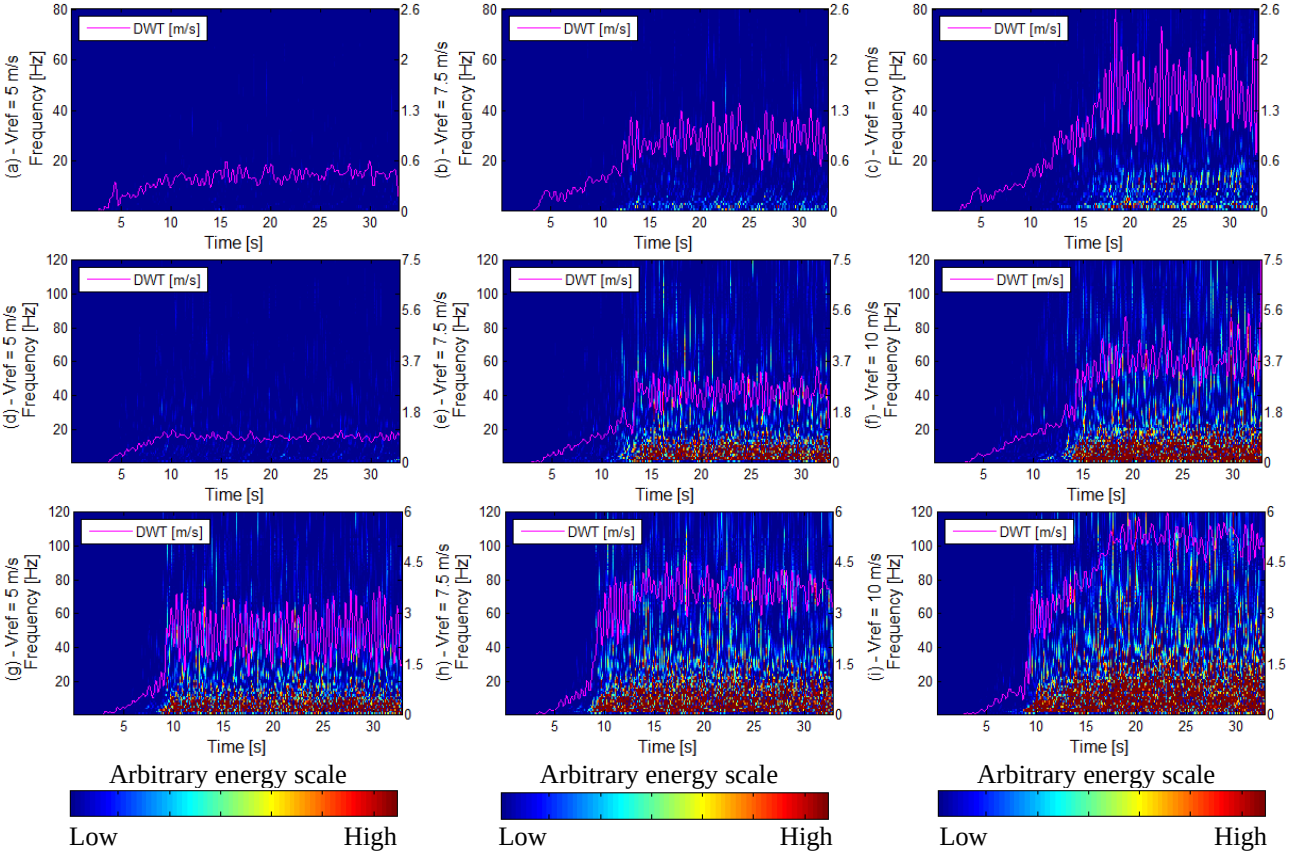

Figure 4 – Continuous wavelet transform (CWT). No obstacles case: 5 m/s (a), 7.5 m/s (b) and 10 m/s (c). One obstacle case 5 m/s (d), 7.5 m/s (e) and 10 m/s (f). Two obstacles case 5 m/s (g), 7.5 m/s (h) and 10 m/s (i).

In all the charts showed in Figure 4, the high values of energy are related to the high velocity levels presented. The results presented by Habowski, 2020, showed that the energy content is more influenced by the velocity fluctuations than the velocity levels. Therefore, in this work, the velocity fluctuations are more intense for high velocity levels. This combination leads to higher levels of energy when the velocity achieves its stabilization.

No obstacles case (Figure 4 a–c) presents the lowest values of energy, where high energy levels are observed only for the case of 10 m/s. With one obstacle (Figure 4 d–f), the energy levels increase, as the consequence of the higher free-flow velocity. For two obstacles (Figure 4 g–i), the high levels of energy are present even in the lowest velocity proposed (5 m/s, Figure 4 g). This case also present higher levels of energy in about 20 Hz, which is higher than the one obstacle case, about 15 Hz.

4.3 Position behavior analysis

The angular position results for all the experiments are presented in Figure 5, where the angular position (y-axis, rad) is plotted in function of the time step (x-axis, s). The video recordings are synchronized with the velocity series. The main and common characteristic of these experiments is that they start from zero rad (rest position) and increase its angular position until it achieves the maximum value in the specific experiment. During the noticeable increase of the angular position, the values alternates between positive and negative values, as expected. This characteristic of the oscillatory movement by the setup was presented in all experiments. These oscillations disturb the velocity downstream the cylinders, as observed in Figure 3, after 12s.

In the no obstacles case (Figure 5a), the maximum angular positions were – 0.025, – 0.040, and – 0.045 rad for reference flow velocities of 5, 7.5 and 10 m/s, respectively. In this case, the angular amplitudes are very small, the shedding energy is not enough to displace the setup (Figure 4 a-c).

For the case with one obstacle (Figure 5b) the angular positions presented values that did not oscillate between the rest position (zero rad). The mean value of angular displacement is deviated by – 0.142 rad due the fact that the obstacle

inserted in this experiment deviates the flow to one side. As consequence, the obstacle forces the setup to oscillate in this form. The maximum angular positions achieved in this case are – 0.185, – 0.559 and – 0.583 for velocities of 5, 7.5 and 10 m/s, respectively.

Finally, for the last case (Figure 5c), the setup achieves the highest angular positions among the previous geometrical configurations: – 0.487, – 0.614 and – 0.652 rad for 5, 7.5 and 10 m/s, respectively. In this case, a high blockage ratio is imposed close to the cylinders. As consequence, the flow is accelerated, and higher angular positions and velocity values are presented.

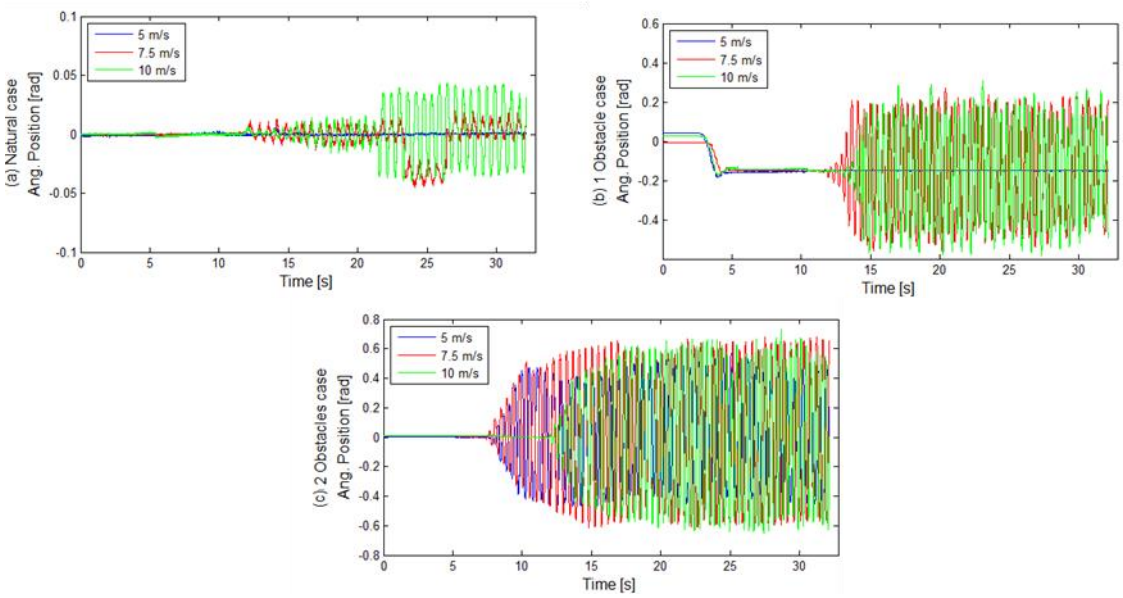

Figure 5 - Angular position analysis for the experiments and velocities proposed in this work: no obstacles case (a), 1 obstacle case (b) and 2 obstacles case (c).

Previous studies exploring tandem configurations showed that the main mechanism which may disturb the downstream cylinder is the vortex shedding from the upstream cylinder (Alam and Zhou, 2008; Habowski et al., 2020). When the downstream cylinder is not fixed, the vortex shedding from the upstream cylinder may displace the downstream cylinder according to the setup degrees of freedom. In the case of this study, the system only allows rotational displacement. Thus, considering the results of Figure 5, the vortex shedding from upstream cylinder only had energy ot make the system oscillate. Even though the oscillatory behavior was expected, the levels achieved by the system were unknown and depended on many factors such as *p/d* ratio, reference flow velocity, damping of the system, blockage ratio, and others. The observed oscillations could allow the possibility of energy extraction from vortex shedding, expanding the use of this phenomenon.

5. CONCLUDING REMARKS

This article presented an experimental study about two circular cylinders placed in a setup free to oscillate, inside an aerodynamic flow channel, with *p/d* relation of 1.26. Results were shown involving velocity behind the downstream cylinder, its reconstruction by means of discrete wavelets, energy content analysis by means of continuous wavelets and angular position behavior. The results were evaluated from the signals collected by the hot wire anemometers technique, being posteriorly analyzed by Matlab software. The Tracker software was employed to perform the video recording study and identify the angular behavior of the setup.

Velocity results showed several oscillations in the signals, due to the oscillatory movements presented in the angular position analysis results. Also, low levels of velocity were presented in the no obstacles case in comparison of the cases with one and two obstacles. These higher levels were expected, since the blockage ratio is increased with the obstacles, accelerating the flow close to the cylinders.

The energy content analysis showed energy concentration in the same time stamp when the velocity was increased. The flow energy is more influenced by the velocity fluctuations than the energy levels for the cases studied in this work (Habowski et al., 2020). Therefore, in this work, the velocity levels were increased together with the velocity fluctuation, which pointed out the high energy levels in presented results.

To finish the exploration, the angular position analysis showed the oscillatory behavior of the system. The case with one obstacle presented a deviation in the mean value of angular displacement. The no obstacles case showed low levels

of oscillation, while the case with two obstacles achieved the highest angular positions in comparison of the other experiments.

It is well established that the main mechanism that disturbs and make the system oscillate is the vortex shedding from the upstream cylinder, a fact which was corroborated in the results observed in this work. The oscillatory behavior in observed levels can be broadly explored for extraction of energy. Future works contemplating new experiments and a wider mathematical exploration will be carried out.

6. ACKNOWLEDGEMENTS

This study was financed in part by the Coordenação de Aperfeiçoamento de Pessoal de Nível Superior - Brasil (CAPES) - Finance Code 001.

7. REFERENCES

Alam, M.M., Moriya, M. and Sakamoto, H., 2002. "Aerodynamic characteristics of two side-by-side circular cylinders and application of wavelet analysis on the switching phenomenon". *Journal of Fluids and Structures*, v. 18, n. 3–4, p. 325–346.

Alam, M.M. and Sakamoto, H., 2005. "Investigation of Strouhal frequencies of two staggered bluff bodies and detection of multistable flow by wavelets". *Journal of Fluids and Structures*, v. 20, n. 3, p. 425–449.

Alam, M.M and Zhou, Y., 2008. "Strouhal numbers, forces and flow structures around two tandem cylinders of different diameters". *Journal of Fluids and Structures*, v. 24, p. 505–526.

Bao, Y., Huang, C., Zhou, D., Tu, J. and Han, Z., 2012. "Two-degree-of-freedom flow-induced vibrations on isolated and tandem cylinders with varying natural frequency ratios". *Journal of Fluids and Structures*, v. 35, p. 50–75.

Blevins, R.D., 1990. *Flow-induced vibration*. Van Nostrand Reinhold, 2nd edition.

Chen, S.S., 1987. *Flow-induced vibration of circular cylindrical structures*. Washington, United Stares.

Chen, S.S., 1987. "A general theory for dynamic instability of tube arrays in crossflow". *Journal of Fluids and Structures*, v. 1, p. 35–53.

De Paula, A.V., Endres, L.A.M. and Möller, S.V., 2012. "Bistable features of the turbulent flow in tube banks of triangular arrangement". *Nuclear Engineering and Design*, v. 249, p. 379–387.

De Paula, A.V., Endres, L.A.M. and Möller, S.V., 2013. "Experimental study of the bistability in the wake behind three cylinders in triangular arrangement". *Journal of the Brazilian Society of Mechanical Sciences and Engineering*, v. 35, n. 2, p. 163–176.

Endres, L.A.M. and Möller, S.V., 2001. "On the fluctuating wall pressure field in tube banks". *Nuclear Engineering and Design*, v. 203, n. 1, p. 13–26.

Gu, Z., 1996. "On interference between two circular cylinders at supercritical Reynolds number". *Journal of Wind Engineering and Industrial Aerodynamics*, v. 62, p. 175–190.

Habowski, P.B, De Paula, A.V., Möller, S.V., 2019. "Analysis of the wake of two parallel circular cylinders at several angular positions to the flow". In *Proceedings of the 25th International Congress of Mechanical Engineering – COBEM 2019*. Uberlândia, Brazil.

Habowski, P.B., 2020. *Analysis of the power generated by the bistable flow around circular cylinders*. Master's degree thesis, Universidade Federal do Rio Grande do Sul, Porto Alegre – RS, Brasil.

Habowski, P.B, De Paula, A.V., Möller, S.V., 2020. "Wake behavior analysis for two circular cylinders placed at several angles to the flow". *Journal of the Brazilian Society of Mechanical Sciences and Engineering*, v.82, p. 441.

Indrusiak, M.L.S., Kozakevicius, A.J. and Möller, S. V., 2016. "Wavelet Analysis Considerations for Experimental Nonstationary Flow Phenomena". *Revista de Engenharia Térmica*, v. 15, n. 1, p. 67.

Jenkins, L.N., Khorrami, M.R., Choudari, M.M and McGinley, C.B., 2005. "Characterization of unsteady flow structures around tandem cylinders for component interaction studies in airframe noise". In *Proceedings of the 11th AIAA/CEAS Aeroacoustics Conference (26th AIAA Aeroacoustics Conference)*, Monterey – California, EUA.

Jenkins, L.N., Neuhart, D.H., McGinley, C.B., Choudari, M.M and Khorrami, M.R., 2006. "Measurements of unsteady wake interference between tandem cylinders". In *Proceedings of the 36th AIAA Fluid Dynamics Conference and Exhibit*, San Francisco – California, EUA.

Lockard, D.P., Khorrami, M.R., Choudhari, M.M., Hutcheson, F.V. and Brooks, T.F., 2007. "Tandem Cylinder Noise Predictions". In *Proceedings of 13th AIAA/CEAS Aeroacoustics Conference (28th AIAA Aeroacoustics Conference)*, Rome, Italy.

Neumeister, R.F., Petry, A.P. and Möller, S.V., 2018. "Characteristics of the wake formation and force distribution of the bistable flow on two cylinders side-by-side". *Journal of the Brazilian Society of Mechanical Sciences and Engineering*, v. 40, n. 12, p. 1–19.

Païdoussis, M.P., 1980. "Flow-induced vibrations in nuclear reactors and heat exchangers: practical experiences and state of knowledge". In *Proceedings of Practical experiences with flow-induced vibrations, 1979*. Springer-Verlag, Berlin, pp. 1–81.

Païdoussis, M.P, 1982. "A review of flow-induced vibrations in reactors and reactor components". *Nuclear Engineering and Design*, v. 74, p. 31–60.

Papaioannou, G., Yue, D., Triantafyllou, M. and Karniadakis, G.E., 2006. "Three-dimensionality effects in flow around two tandem cylinders". *Journal of Fluid Mechanics*, v. 558, p. 387–413.

Papaioannou, G., Yue, D., Triantafyllou, M. and Karniadakis, G.E., 2008. "On the effect of spacing on the vortex-induced vibrations of two tandem cylinders". *Journal of Fluids and Structures*, v. 24, p. 833–854.

Percival, D.B. and Walden, A.T., 2000. "Wavelet Methods for Time Series Analysis". *Cambridge University Press.*

Qin, B., Alam, M.M. and Zhou, Y, 2017. "Two tandem cylinders of different diameters in cross-flow: Flow-induced vibration". *Journal of Fluid Mechanics*, v. 829, p. 621–658.

Sumner, D., Price, S.J. and Païdoussis, M.P., 1999. "Tandem Cylinders in Impulsively Started Flow". *Journal of Fluids and Structures*, v. 13, n. 7–8, p. 955–965.

Sumner, D., Price, S.J. and Païdoussis, M.P, 2000. "Flow-pattern identification for two staggered circular cylinders in cross-flow". *Journal of Fluid Mechanics*, v. 411, p. 263–303.

Sumner, D., Price, S.J. and Païdoussis, M.P., 1997. "Investigation of impulsively-started flow around side-by-side circular cylinders: Application of particle image velocimetry". *American Society of Mechanical Engineers, Aerospace Division (Publication) AD*, v. 53–1, p. 93–102.

Tennekes, H and Lumley, J.L., 1972. "A First Course in Turbulence". The MIT Press.

Varela, D., Neumeister, R.F., Dias, G., De Paula, A.V. and Möller, S.V., 2017. "Experimental analysis of turbulent transversal flow on two fixed parallel cylinders with oscillatory and rotational freedom". In *Proceedings of COBEM 2017 – 24th International Congress of Mechanical Engineering. Curitiba, PR – Brazil.*

Woyciekoski, M.L., Endres, L.A.M., De Paula, A.V. and Möller, S.V., 2020. "Influence of the free end flow on the bistability phenomenon after two side by side finite height cylinders with aspect ratios of 3 and 4 and high blockage". *Ocean Engineering*, v. 195.

Zdravkovich, M.M., 1987. "The effects of interference between circular cylinders in cross flow". *Journal of Fluids and Structures*, v. 1, p. 239–261.

Zhou, Yu and Alam, M.M. "Wake of two interacting circular cylinders: A review". *International Journal of Heat and Fluid Flow*, v. 62, p. 510–537.

8. RESPONSIBILITY NOTICE

The authors are the only responsible for the printed material included in this paper.